Capillary Electrophoresis for Diastereomers of (*R,S*)-Tetrahydroisoquinoline-3-Carboxylic Acid Derivatized with (*R*)-4-Nitro-7-(3-Aminopyrrolidin-1-yl)-2,1,3-Benzoxadiazole: Effect of Molecular Geometries

Zhe Quan, Yaru Song, Andrea Saulsberry, Yinghong Sheng, and **Yi-Ming Liu***
Department of Chemistry, Jackson State University, 1400 Lynch St., Jackson, MS 39217

Abstract

Diastereomers derived from (*R,S*)-tetrahydroisoquinoline-3-carboxylic acid (Tic), a potential neurotoxin with a chiral fluorescence tagging reagent, (*R*)-4-nitro-7-(3-aminopyrrolidin-1-yl)-2,1,3-benzoxadiazole (NBD-APy), are well resolved by capillary electrophoresis (CE). For a better understanding of the separation mechanism, a semiempirical computational method (i.e., AM1 method) is used to study the molecular geometry, relative energy, and size of the derivatives. The molecular sizes are estimated to be 216.3 and 240.6 cm^3/mol for (*R*)-NBD-APy-(*R*)-Tic and (*R*)-NBD-APy-(*S*)-Tic, respectively. The CE elution order of the diastereomeric derivatives confirms the AM1 computational results: (*R*)-NBD-APy-(*R*)-Tic elutes before (*R*)-NBD-APy-(*S*)-Tic. The effects of running buffer pH and the addition of a chiral selector, β-cyclodextrin (β-CD), on the separation are studied. In the presence of β-CD, the migration behavior of the diastereomers is changed because of the formation of CD inclusion complexes. Study of the space-filling models for optimized conformations of the diastereomeric derivatives and β-CD suggests that the geometries of the diastereomers decides that the diastereomers are incorporated into the CD cavity to form CD inclusion complexes with different volumes. Experimental results from CE separations conclude the same.

Introduction

Study of the neurotoxicity of tetrahydroisoquinoline (TIQ) derivatives has been extensive, particularly since the discovery of 1[N]-methyl-4-phenyl-1,2,3,6-tetrahydropyridine's damaging effects on nervous systems (1–4). Dopamine-derived TIQs including salsolinol (Sal) have been found cytotoxic to rat PC 12 cells (5) and human dopaminergic SH-SY5Y cells (6). There is growing evidence indicating that in vivo formation of certain TIQs may be related to alcohol addiction (7,8). Many chiral TIQ molecules have been shown to exhibit enantioselective neurotoxicity (9,10). *N*-Methyl-(*R*)-Sal was found to be much more potent than its optical antipode in inducing apoptosis in dopaminergic neuroblastoma SH-SY5Y cells (11). After being administered into the striatum, the (*R*)-enantiomer of *N*-methyl-Sal induced Parkinsonism in rats, but the (*S*)-enantiomer did not (12). It was shown that endogenous TIQ formation and TIQ N-methylation involved a stereoselective enzymatic process (13). Actually, an enzyme that enantioselectively synthesized (*R*)-Sal has been isolated from rat brain (14).

In our recent efforts to separate TIQ enantiomers using cyclodextrin-modified capillary electrophoresis (CE), no enantiomeric resolution was achieved for a group of highly hydrophilic TIQ derivatives, including (*R,S*)-tetrahydroisoquinoline-3-carboxylic acid (Tic). This problem was solved by employing precolumn derivatization with a chiral fluorescence tagging reagent, (*R*)-4-Nitro-7-(3-aminopyrrolidin-1-yl)-2,1,3-benzoxadiazole (NBD-APy). The diastereomers derived from Tic were well resolved by CE. For a better understanding of the separation mechanism, a semiempirical computation method (i.e., AM1 method) was used to optimize the molecular geometries of the diastereomeric derivatives, and the molecular sizes were then estimated. The computational studies predicted significant differences in molecular sizes for these diastereomers. The results were confirmed by CE separations.

CE separations of diastereomers have been reported (15–21). Schuetzner et al. described CE separations of diastereomers derived from amino acids with (+)-*O,O*'-dibenzoyl-L-tartaric anhydride and studied the effects of pH, solvent composition, and the addition of polymer additives on such separations (20,21). In the present work, the emphasis was placed on the effect of molecular geometry, and related molecular size, on CE diastereomer separation.

*Author to whom correspondence should be addressed: email yiming.liu@jsums.edu.

Experimental

Chemicals

Tic, β-cyclodextrin (β-CD), triphenylphosphine (TPP), and 2,2'-dipyridyl disulphide (DPDS) were purchased from Sigma-Aldrich (St. Louis, MO). (*R*)-4-Nitro-7-(3-aminopyrrolidin-1-yl)-2,1,3-benzoxadiazole ((*R*)-NBD-APy) was synthesized according to the procedure described by Toyo'oka et al. (22). All other chemicals were of analytical grade. Milli-Q (Millipore, Milford, MA) water was used throughout.

Apparatus

CE was carried out using a laboratory-built system. The high voltage supply (0–30 kV, Glassman High Voltage, Whitehouse Station, NJ) was used for the driving force. A fused-silica capillary with an effective length of 50 cm and a 50-µm i.d. (Supelco, Bellefonte, PA) was used for all separations. Samples were manually injected into the capillary by hydrodynamic flow for 15 s, with a height difference of 20 cm for the two ends of the capillary. The voltage imposed across the capillary was 20 kV. A lab-built lazer-induced fluorescence detector described previously (23) was used for the detection. The 457.9 nm line from an argon lazer (Innova 90C FreD, Coherent, Santa Clara, CA) was employed for excitation. Fluorescence emission was collected through a 495-nm cut-off optical filter (GG495, Melles Griot, Irvine, CA).

Mass spectrometry (MS) measurements were performed with a Thermo Finnigan LCQ DUO MS (Thermo Finnigan, San Jose, CA). The MS was equipped with an electrospray ionization source operated in the positive ion mode. Samples were infused into the MS using the attached syringe pump at a flow rate of 5 µL/min. The operation conditions were as following: sheath gas flow, 20 arbitrary units; auxiliary gas flow, 0 arbitrary units; spray voltage, 4.5 kV; and heated capillary temperature, 200°C. Relative collision energy of 25% was used for MS^2 (MS–MS) experiments with an isolation width of 3.0 µm. Other parameters were optimized by the automatic tune program. An Xcalibur software package (Thermo Finnigan) was used to process data.

Preparation of diastereomers

A CH_3CN solution containing Tic (0.5mM), (*R*)-NBD-APy (2.0mM), DPDS (2.0mM), and TPP (2.0mM) was prepared and the mixture was vortexed. The derivatization reaction was allowed to proceed for 2 h at room temperature, and the derivative solution was then diluted with acetonitrile to an appropriate concentration for CE separations or MS analyses.

Results and Discussion

Separation of (*R*)-NBD-APy derivatized (*R,S*)-Tic

Derivatization of Tic with NBD-APy is illustrated in Figure 1. MS measurements confirmed that NBD-APy-Tic was the major product from the reaction. The $(M+1)^+$ ion (*m/z* 409) was observed as shown in Figure 2A. The MS–MS of this ion shown in Figure 2B further confirmed the chemical structure. The $(M+1–NO_2)^+$ ion (*m/z* 363) from the fragmentation of NBD-APy-Tic was the major product ion. Nearly identical MS and MS–MS spectra were obtained for the diastereomers. NBD-APy-Tic was highly fluorescent (λ_{ex} = 470 nm and λ_{em} = 540 nm). The 457.9-nm line from an argon lazer is very close to 470 nm; therefore, it is well suited for the excitation.

As illustrated in Figure 3, (*R*)-NBD-APy derivatized (*R,S*)-Tic were well resolved by CE using a 50mM phosphate buffer at pH 3.0, with (*R*)-NBD-APy-(*R*)-Tic migrating faster than (*R*)-NBD-APy-(*S*)-Tic. Movement of a molecule in CE is governed by elec-

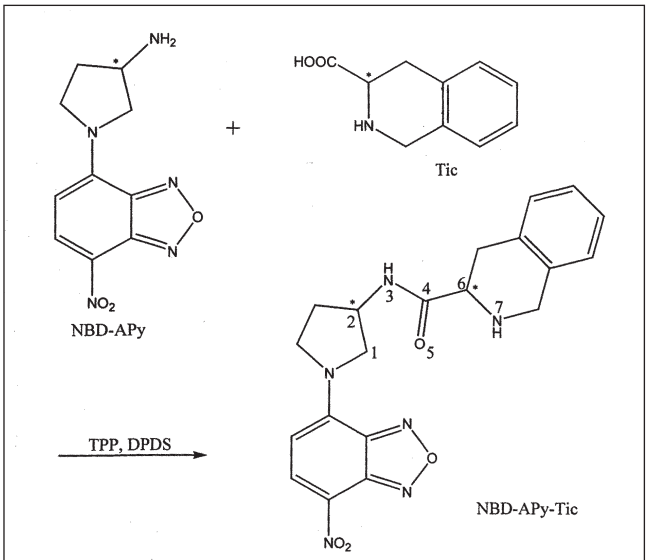

Figure 1. Formation of diastereomers. Tic reacts with NBD-APy in the presence of TPP and DPDS, DPDS as catalysts.

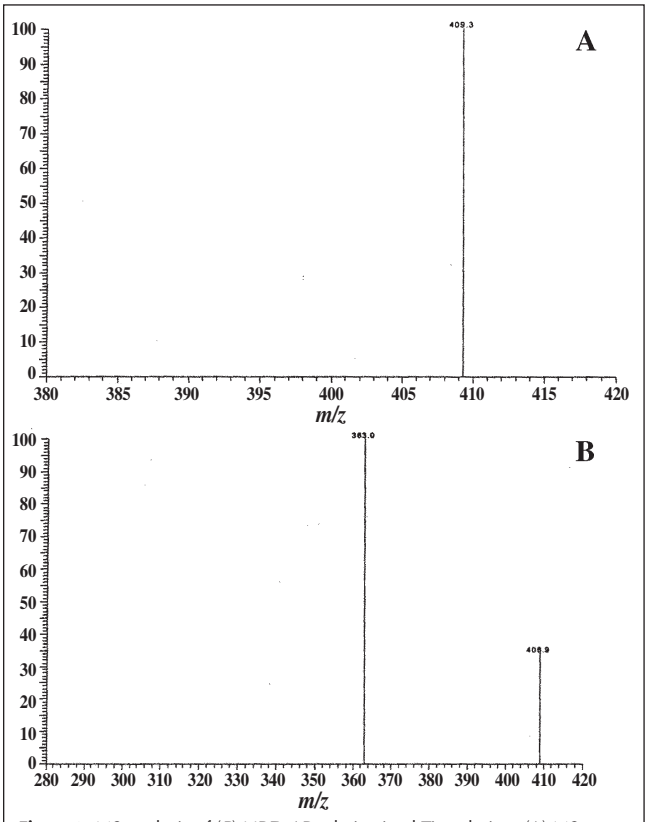

Figure 2. MS analysis of (*R*)-NBD-APy derivatized Tic solution: (A) MS spectrum of (*R*)-NBD-APy-Tic; (B) MS–MS of *m/z* 409 $(M+1)^+$ ion from A. The formula weight of NBD-APy-Tic is 408.

troosmotic (EO) mobility (μ_{eo}) and electrophoretic mobility (μ_{em}) (24):

$$\mu = \mu_{eo} + \mu_{em} = \varepsilon\zeta/\eta + q/6\pi\eta r \qquad \text{Eq. 1}$$

where μ represents the mobility of a molecule, ε stands for the dielectric constant, ζ indicates the zeta potential of the liquid–solid interface, η is the viscosity of the buffer solution, and *q* and *r* stand for the net charge and ionic radius, respectively.

Because the diastereomers were in the same CE system, they had the same μ_{eo} value. Therefore, the charge to size ratio in the term of μ_{em} determines the mobility according to equation 1. Although at pH 3.0 the diastereomers may be protonated to a similar level, their molecular sizes can be different because their steric structures are different. In this work, a computational method was used to explore the size differences for diastereomers. The geometries of the diastereomeric derivatives were optimized by means of the Berny method (25) at the semiempirical AM1 level (26–28). Various conformations of each compound have been investigated as rotations of the C_2–N_3, N_3–C_4, and C_4–C_6 bonds can lead to different conformations (see Figure 1 for position assignments). However, these conformations exist at different energy levels. It was found that the orientations of the NBD-APy and the TIQ moieties had the most important impact on the stabilities of NBD-APy-Tic diastereomeric molecules. For instance, the NBD-APy and TIQ moieties can have either cis- or trans-configurations, and thus the dihedral angle of the two moieties can be around 0° or 180°. Take an (*R*)-NBD-APy-(*R*)-Tic molecule as an example. In the optimized geometry (shown in Figure 4), the dihedral angles of C_1–C_2–N_3–C_4, C_2–N_3–C_4–O_5 and C_2–N_3–C_4–C_6, N_3–C_4–C_6–N_7 are 128.9°, –3.8°, 178.1°, and 61.8°, respectively, versus –72.3°, 0.9°, 178.7°, and –170.7°, respectively, in an alternative geometry. However, the alternative conformation was found to be less stable than the optimized one by approximately 3.27 kcal/mol. From the conformations studied, only those with the lowest relative energy are selected for further studies. The corresponding parameters for the diastereomeric derivatives are listed in Table I. The volumes and radii of the four geometries were computed using the keyword volume, which was implemented in the Gaussian 94 program (29). As can be seen, the molecular sizes of the diastereomers are significantly different, which means these diastereomers can be separated effectively by CE, according to equation 1. Actually, the computational results properly explain the migration behavior of the diastereomers in CE (as shown in Figure 3): (*R*)-NBD-APy-(*R*)-Tic elutes before (*R*)-NBD-APy-(*S*)-Tic because (*R*)-NBD-APy-(*R*)-Tic is smaller. Although the molecular sizes shown in Table I are for molecules in a gaseous phase, they can be used for a comparison because the diastereomers are hydrated similarly in the same solution.

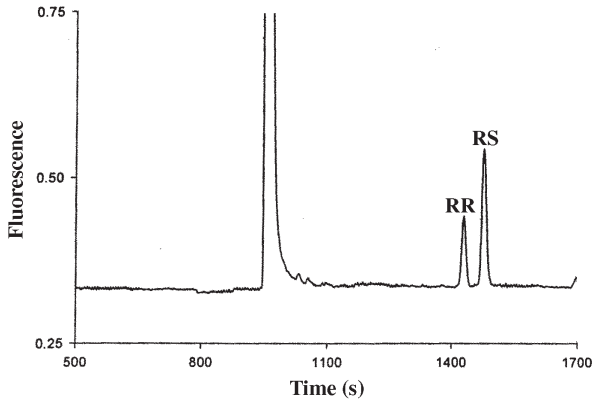

Figure 3. Electropherogram for separation of NBD-APy-(*R,S*)-Tic diastereomers. *RR*, (*R*)-NBD-APy-(*R*)-Tic (25μM); *RS*, (*R*)-NBD-APy-(*S*)-Tic (50μM). Peaks were identified by spiking. Voltage applied was 20 kV. Running buffer contained 50mM phosphate at pH 3.0. Capillary effective length and i.d. were 50 cm and 50 μm, respectively.

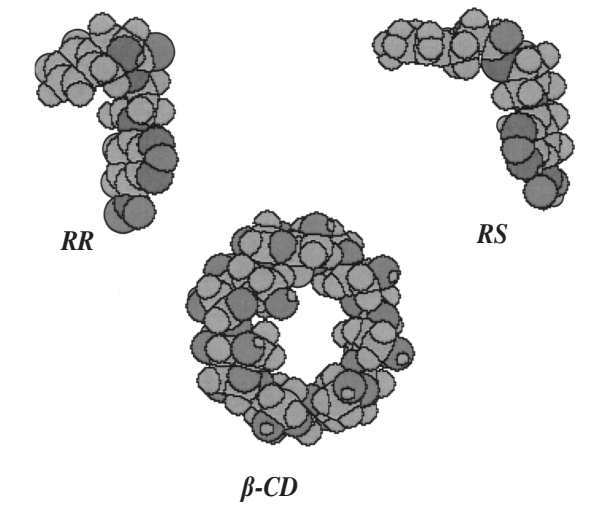

Figure 4. Space-filling models for the optimized conformations of (*R*)-NBD-APy-(*R,S*)-Tic diastereomeric derivatives and β-CD. *RR*, (*R*)-NBD-APy-(*R*)-Tic; *RS*, (*R*)-NBD-APy-(*S*)-Tic.

Influence of pH

Influence of running buffer pH on the resolution of (*R*)-NBD-APy derivatized Tic enantiomers was investigated over a pH range from 1.5 to 8.0. The results are shown in Figure 5. As can be seen in acidic running buffers (pH ≤ 5), the diastereomers were well resolved. However, when the pH increased to 6 or higher, no resolution was obtained. Various buffer systems including phosphate, formate, acetate, and borate were tested with similar results. In acidic solutions, the derivatives are protonated and, therefore, positively charged. However, at increased pH values, the diastereomers become electrically neutral, and as a result the value of μ_{em} in equation 1 becomes zero. Thus, $\mu = \mu_{eo}$. Under

Table I. Computational Results for NBD-APy-Tic Diastereomeric Derivatives*

Molecule	Volume (cm^3/mol)	Radius (Å)	Relative energy (kcal/mol)
(*R*)-NBD-APy-(*R*)-Tic	216.3	5.35	0.51
(*R*)-NBD-APy-(*S*)-Tic	240.6	5.53	0.00

* The geometries were optimized with the AM1 method (see text for details).

such conditions, the diastereomers coeluted out along with the EO flow, consequently, no separation could be achieved. Although the effects of ionic strength variation were not taken into consideration in these studies, the observations led to the conclusion that it was necessary to make the diastereomers positively charged in an acidic running buffer in order to resolve them.

Effects of β-CD

The effects of β-CD, a commonly used chiral selector, on the resolution of the diastereomers were investigated. In the presence of β-CD, the migration times of the diastereomers increased significantly. This can be partly attributed to an increase of viscosity caused by β-CD and partly to the formation of β-CD inclusion complexes resulting in an increased molecular size. It should be noted that the elution order of (*R*)-NBD-APy-derived Tic diastereomers shown in Figure 6 was reversed compared with that obtained in Figure 3, in which no β-CD was added. The optimized space-filling models for the diastereomeric derivatives as well as β-CD are shown in Figure 4. β-CD molecules are cyclic polysaccharides consisting of seven α-D-glucose units. A β-CD molecule looks like a truncated hollow cone with a hydrophobic cavity with a diameter of 6.0–6.5 Å (30). Based on the suitable size and steric hindrance, a host β-CD molecule can accommodate a guest NBD-APy-Tic molecule in two ways (31): (*i*) either holding the benzoxadiazole portion equatorially (the axis of the benzoxadiazole is vertical to the long axis of the β-CD cavity) or (*ii*) holding the TIQ portion axially (the axis of the TIQ is parallel to the long axis of the β-CD cavity). As can be seen from the optimized molecular geometries shown in Figure 4, when a complex is formed between (*R*)-NBD-APy-(*S*)-Tic (Figure 4B) and β-CD through either of the two possible portions of the molecule, the other portion of the molecule would cover the inlet of the β-CD like a lid, resulting in a denser inclusion complex with a relatively small bulk. However, this does not apply to the other diastereomeric derivative. When it forms an inclusion complex with β-CD, the remaining portion of the molecule protrudes outside, resulting in larger bulk volume. As a consequence, the smaller (*R*)-NBD-APy-(*S*)-Tic–β-CD complex eluted first.

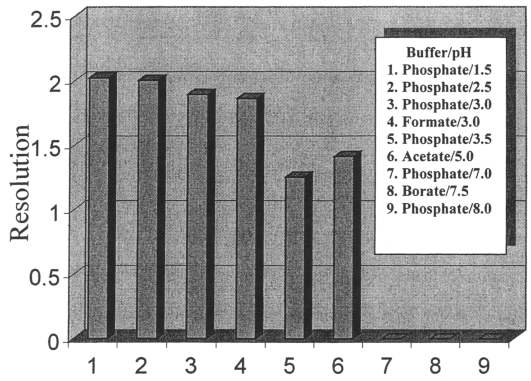

Figure 5. Influence of pH on the separation of (*R*)-NBD-APy-(*R*/*S*)-Tic diastereomers. Concentrations of the buffers were all 50mM. Buffer and pH are indicated in the insert. Resolution is calculated as $R_s = 2(R_2 - R_1)/(W_1 + W_2)$, where $(R_2 - R_1)$ represents the difference of migration times for two solutes, W_1 and W_2 are widths of the corresponding peaks. CE conditions were as in Figure 3.

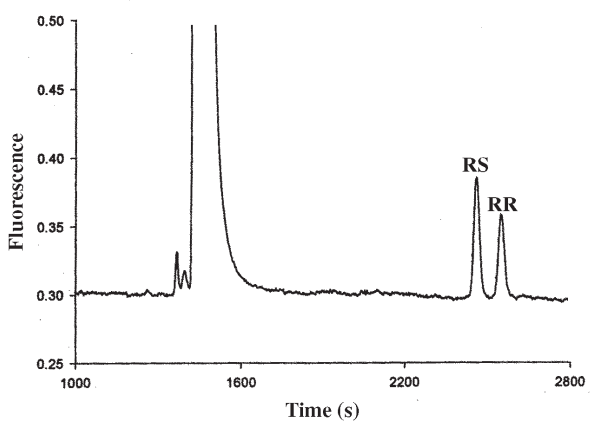

Figure 6. Effects of β-CD on the separation of (*R*)-NBD-APy-(*R,S*)-Tic diastereomers. *RR*, (*R*)-NBD-APy-(*R*)-Tic (20μM); *RS*, (*R*)-NBD-APy-(*S*)-Tic (25μM). Running buffer contained 50mM phosphate (pH 3.0) and 12mM β-CD. Other conditions were the same as in Figure 3.

Conclusion

Chiral separation of (*R,S*)-Tic, a potential neurotoxin, has been achieved. The method is based on the CE separation of the diastereomers derived with a chiral fluorescence tagging reagent, (*R*)-NBD-APy. Theoretical calculations using a semiempirical method (i.e., AM1 method) have shown that the differences in molecular sizes of the diastereomers play a pivotal role in the separation. Introduction of β-CD into the CE running buffer (50mM phosphate buffer at pH 3.0) reversed the migration order of the diastereomers. Because their relative sizes were changed, their steric geometries caused differences in the sizes of the inclusion complexes between NBD-APy derivatives and β-CD molecules.

Acknowledgments

Support from NIH grants (NS44177, G12RR12459, and S06GM08047) is gratefully acknowledged.

References

1. T. Nagatsu. Isoquinoline neurotoxins in the brain and Parkinson's disease. *Neurosci. Res.* **29:** 99–111 (1997).
2. T. Nagatsu. Amine-related neurotoxins in Parkinson's disease: past, present, and future. *Neurotoxicol. Teratol.* **24:** 565–69 (2002).
3. J. Vetulani, L. Antkiewicz-Michaluk, I. Nalepa, and M. Sansone. A possible physiological role for cerebral tetrahydroisoquinolines. *Neurotox. Res.* **5:** 147–55 (2003).
4. Y. Kotake, S. Ohta, I. Kanazawa, and M. Sakurai. Neurotoxicity of an endogenous brain amine, 1-benzyl-1,2,3,4-tetrahydroisoquinoline in organotypic slice co-culture of mesencephalon and striatum. *Neuroscience* **117:** 63–70 (2003).
5. Y.J. Surh, Y.J. Jung, J.H. Jang, J.S. Lee, and H.R. Yoon. Iron enhancement of oxidative DNA damage and neuronal cell death induced by

salsolinol. *J. Toxicol. Environ. Health A* **65:** 473–88 (2002).
6. S. Shavali, J. Ren, and M. Ebadi. Insulin-like growth factor-1 protects human dopaminergic SH-SY5Y cells from salsolinol-induced toxicity. *Neurosci. Lett.* **340:** 79–82 (2003).
7. R.D. Myers. Tetrahydroisoquinolines and alcoholism: where are we today? *Alcohol.: Clin. Exp. Res.* **20:** 498–500 (1996).
8. M. Jamal, K. Ameno, T. Kubota, S. Ameno, X. Zhang, M. Kumihashi, and I. Ijiri. In vivo formation of salsolinol induced by high acetaldehyde concentration in rat striatum employing microdialysis. *Alcohol Alcohol* **38:** 197–201 (2003).
9. K. Abe, K. Taguchi, T. Wasai, J. Ren, I. Utsunomiya, T. Shinohara, T. Miyatake, and T. Sano. Stereoselective effect of (R)- and (S)-1-methyl-1,2,3,4-tetrahydroisoquinolines on a mouse model of Parkinson's disease. *Brain Res. Bull.* **56:** 55–60 (2001).
10. M. Naoi, W. Maruyama, Y. Akao, and H. Yi. Dopamine-derived endogenous N-methyl-(R)-salsolinol: its role in Parkinson's disease. *Neurotoxicol. Teratol.* **24:** 579–91 (2002).
11. W. Maruyama, A.A. Boulton, B.A. Davis, P. Dostert, and M. Naoi. Enantio-specific induction of apoptosis by an endogenous neurotoxin, N-methyl(R)salsolinol, in dopaminergic SH-SY5Y cells: suppression of apoptosis by N-(2-heptyl)-N-methylpropargylamine. *J. Neural. Transm.* **108:** 11–24 (2001).
12. M. Naoi, W. Maruyama, Y. Dostert, and Y. Hashizume. N-methyl-(R) salsolinol as a dopaminergic neurotoxin: from an animal model to an early marker of Parkinson's disease. *J. Neural Transm. Suppl.* **50:** 89–105 (1997).
13. Th. Muller, S.S. Baum, D. Haussermann, D. Woitalla, H. Rommelspacher, H. Przuntek, and W. Kuhn. Plasma levels of R- and S-salsolinol are not increased in "de-novo" Parkinsonian patients. *J. Neural. Transm.* **105:** 239–46 (1998).
14. M. Naoi, W. Maruyama, P. Dostert, K. Kohda, and T. Kaiya. A novel enzyme enantio-selectively synthesizes (R)salsolinol, a precursor of a dopaminergic neurotoxin, N-methyl(R)salsolinol. *Neurosci. Lett.* **212:** 183–86 (1996).
15. H. Nishi, T. Fukuyama, and M. Matsuo. Resolution of optical isomers of 2,3,4,6-tetra-*O*-acetyl-β-D-glucopyranosyl isothiocyanate (GITC)-derivatized DL-amino acids by micellar electrokinetic chromatography. *J. Microcolumn Sep.* **2:** 234–40 (1990).
16. A.D. Tran, T. Blanc, and E.J. Leopold. Free solution capillary electrophoresis and micellar electrokinetic resolution of amino acid enantiomers and peptide isomers with L- and D-Marfey's reagents. *J. Chromatogr.* **516:** 241–49 (1990).
17. K.C. Chan, G.M. Muschik, and H.J. Issaq. Enantiomeric separation of amino acids using micellar electrokinetic chromatography after precolumn derivatization with the chiral reagent 1-(9-fluorenyl)-ethyl chloroformate. *Electrophoresis* **16:** 504–509 (1995).
18. N. Gel-Moreto, R. Streich, and R. Galensa. Chiral separation of six diastereomeric flavanone-7-O-glycosides by capillary electrophoresis and analysis of lemon juice. *J. Chromatogr. A* **925:** 279–89 (2001).
19. N. Gel-Moreto, R. Streich, and R. Galensa. Chiral separation of diastereomeric flavanone-7-O-glycosides in citrus by capillary electrophoresis. *Electrophoresis* **24:** 2716–22 (2003).
20. W. Schuetzner, S. Fanali, A. Rizzi, and E. Kenndler. Separation of diastereomers by capillary zone electrophoresis with polymer additives: effect of polymer type and chain length. *Anal. Chem.* **67:** 3866–70 (1995).
21. W. Schuetzner, S. Fanali, A. Rizzi, and E. Kenndler. Separation of diastereomers by capillary zone electrophoresis in free solution with polymer additive and organic solvent component. Effect of pH and solvent composition. *J. Chromatogr. A* **719:** 411–20 (1996).
22. T. Toyo'oka, M. Ishibashi, and T. Terao. Fluorescent chiral derivatization reagents for carboxylic acid enantiomers in high-performance liquid chromatography. *Analyst* **117:** 727–33 (1992).
23. S. Zhao, Y. Feng, M. H. LeBlanc, and Y-.M. Liu. Determination of free aspartic acid enantiomers in rat brain by capillary electrophoresis with laser-induced fluorescence detection. *J. Chromatogr. B, Biomed. Appl.* **762:** 97–101 (2001).
24. R. Weinberger. *Practical Capillary Electrophoresis*, 2nd ed. Academic Press, San Diego, CA, 2000.
25. H.B. Schlegel. Optimization of equilibrium geometries and transition structures. *J. Comp. Chem.* **3:** 214–18 (1982).
26. M. Dewar and W. Thiel. Ground states of molecules. 38. The MNDO method. Approximations and parameters. *J. Am. Chem. Soc.* **99:** 4899–4907 (1977).
27. M.J.S. Dewar, M.L. McKee, and H.S. Rzepa. MNDO parameters for third period elements. *J. Am. Chem. Soc.* **100:** 3607 (1978).
28. M.J.S. Dewar, E.G. Zoebisch, E.F. Healy, and J.J.P Stewart. Development and use of quantum mechanical molecular models. 76. AM1: a new general purpose quantum mechanical molecular model. *J. Am. Chem. Soc.* **107:** 3902–3909 (1985).
29. M.J. Frisch, G.W. Trucks, H.B. Schlegel, P.M.W. Gill, B.G. Johnson, M.A. Robb, J.R. Cheeseman, T.A. Keith, G.A. Petersson, J.A. Montgomery, K. Raghavachari, M.A. Al-Laham, V.G. Zakrzewski, J.V. Ortiz, J.B. Foresman, J. Cioslowski, B.B. Stefanov, A. Nanayakkara, M. Challacombe, C.Y. Peng, P.Y. Ayala, W. Chen, M. Wong, J.L. Andres, E.S. Replogle, R. Gomperts, R.L. Martin, D.J. Fox, J.S. Binkley, D.J. Defrees, J.Baker, J.P. Stewart, M. Head-Gordon, C. Gonzalez, and J.A. Pople. Gaussian 94 Revision B.3. Gaussian Inc., Pittsburgh, PA, 1995.
30. J. Szejtli. Introduction and general overview of cyclodextrin chemistry. *Chem. Rev.* **98:** 1743–53 (1998).
31. K.A. Connors. The stability of cyclodextrin complexes in solution. *Chem. Rev.* **97:** 1325–57 (1997).

Manuscript received April 11, 2004;
revision received October 22, 2004.